

Spatial optical solitons in microstructured cavities

O.A. Egorov · R. Iliew · C. Etrich · K. Staliunas ·
F. Lederer

Received: 6 April 2011 / Revised version: 20 May 2011 / Published online: 21 July 2011
© Springer-Verlag 2011

Abstract We present a detailed study of the dynamics of light in passive nonlinear resonators with shallow and deep intracavity periodic modulation of the refractive index in both longitudinal and transverse directions of the resonator. We investigate solutions localized in the transverse direction (so-called Bloch cavity solitons) by means of envelope equations for underlying linear Bloch modes and solving Maxwell's equations directly. Using a round-trip model for forward and backward propagating waves we review different types of Bloch cavity solitons supported by both focusing (at normal diffraction) and defocussing (at anomalous diffraction) nonlinearities in a cavity with a weak-contrast modulation of the refractive index. Moreover, we identify Bloch cavity solitons in a Kerr-nonlinear all-photonic crystal resonator solving Maxwell's equations directly. In order to analyze the properties of Bloch cavity solitons and to obtain analytical access we develop a modified mean-field model and prove its validity. In particular, we demonstrate a substantial narrowing of Bloch cavity solitons near the zero-diffraction regime. Adjusting the quality factor and resonance frequencies of the resonator optimal Bloch cavity solitons in terms of width and pump energy are identified.

1 Introduction

Passive planar resonators with a nonlinear optical response are known to exhibit many important and fundamental effects such as optical bistability, modulational (spatial) instability, and spatial pattern formation [1–4]. They can also support spatially localized nonlinear modes, so-called cavity solitons (CS) [4–10]. Cavity solitons are either associated with locked switching waves between two stable homogeneous solutions [7] or appear near a region of modulational instability of these homogeneous solutions [8]. Because of the permanent energy exchange between an external pump and intrinsic losses they belong to the general class of dissipative solitons [11] and are therefore strong attractors. Thus they can be excited from a wide range of initial conditions, the basin of attraction. Illuminating a resonator by a plane holding beam, CSs appear as spatially localized domains in the reflected or transmitted fields, which are “switched up” or “switched down” for bright or dark CSs, respectively. The properties of CSs have been studied both theoretically and experimentally during the last two decades (for reviews see [4, 7, 8, 10]).

In accordance with the general paradigm of spatial soliton formation the diffraction of waves has to be compensated by the nonlinear frequency shift. Therefore the crucial linear parameter which determines the existence range of CSs and their properties is the net diffraction of the resonator. Bright CSs exist for focusing nonlinearities combined with normal (positive) diffraction. In mean-field models the CS size directly scales with the square root of the diffraction coefficient. Thus the potential applications of CSs in optical memory or optical routing devices [10] depend crucially on the strength of diffraction, and their applicability can be strongly improved by a proper diffraction management. For instance, the strength of diffraction can be

O.A. Egorov (✉) · R. Iliew · C. Etrich · F. Lederer
Institute of Condensed Matter Theory and Solid State Optics,
Friedrich-Schiller-Universität Jena, Max-Wien-Platz 1,
07743 Jena, Germany
e-mail: oleg.egorov@uni-jena.de

K. Staliunas
Institució Catalana de Recerca i Estudis Avançats (ICREA),
Departament de Física i Enginyeria Nuclear,
Universitat Politècnica de Catalunya, Colom 11, 08222 Terrassa,
Barcelona, Spain

reduced theoretically to arbitrarily small values by inserting a layer of left-handed materials (LHM) in the cavity of an optical microresonator [12]. In this case the inherent non-locality of LHMs can significantly change the properties of CSs setting a new minimal size limit [13]. A more realistic possibility for diffraction management is to employ photonic structures with a spatially modulated refractive index such as photonic lattices and crystals [14–16] which, among other properties, allow the modification of the net diffraction of the propagating light beams. Diffractionless propagation of narrow beams in periodic photonic structures (PPSs) was demonstrated [17–19]. The modulation of the refractive index was shown to modify also the nonlinear light propagation, including the generation of different types of conservative spatial solitons for both focusing and defocussing nonlinearities [16, 20, 21], and also at the zero-diffraction point [22].

The manipulation of diffraction was readily utilized in dissipative systems, too. Even in the simplest case of a one-dimensional shallow modulation of the refractive index new important effects were predicted. The modulation can modify and even inhibit modulational instability in nonlinear resonators as proposed in [23, 24] and as recently studied experimentally in dissipative feedback systems [25]. The formation of discrete CSs [26, 27], lattice-CSs and multi-band lattice-CSs [28] were predicted for a modulation of the refractive index in one transverse direction. Dissipative Bragg solitons [29, 30] are possible, provided that the index is modulated in the direction of light propagation, i.e., in the longitudinal direction. In the intermediate case, i.e., if the light propagates at an angle with respect to the modulation direction, a special class of dissipative solitons, so-called mid-band solitons, were found. These solitons have no counterparts in conservative systems and were shown to exist in lasers with a periodic lateral modulation of the refractive index [31, 32] and in arrays of coupled Kerr-nonlinear cavities [33].

Diffraction manipulation in nonlinear dissipative systems was studied more extensively for one-dimensional modulations. Recently it was proposed to combine these approaches and to consider the propagation of light in nonlinear media with a weak-contrast modulation in both longitudinal and transverse directions [34, 35]. This allowed merging of two areas, diffraction management of two-dimensional (2D) Bloch waves and dissipative solitons in nonlinear resonators. Note that only linear properties of such resonators have been considered experimentally so far [36, 37].

In this paper we review our recent results on the dynamics of light in passive nonlinear resonators with a periodic modulation of the refractive index both in longitudinal and transverse direction of the resonator (2D periodic photonic structure). We consider two possible configurations of the intracavity PPS. One of them is a nonlinear resonator with a

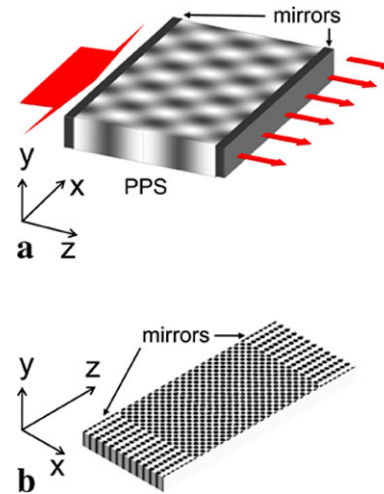


Fig. 1 (a) A nonlinear resonator with an intracavity 2D weak-contrast periodic photonic structure. (b) Geometry of the all-photonic crystal resonator

shallow (weak-contrast) periodic modulation of the refractive index [Fig. 1(a)]. It serves as a starting point for understanding the fundamental physics of nonlinear localization in terms of Bloch modes. This system is described by means of a paraxial round-trip model based on plane waves with the modulation as a perturbation (see Sect. 2). In Sect. 3 a generalized mean-field approach is introduced, accounting also for higher-order diffraction terms. The existence of localized states or Bloch cavity solitons (BCSs) is discussed in Sect. 4.

The second configuration, a Kerr-nonlinear all-photonic crystal Fabry-Pérot resonator [38] with a high-index contrast [Fig. 1(b)], is introduced in Sect. 5. In order to exploit the diffraction management at most, in Sect. 6 we study the light dynamics in this system, where the strong index modulation is on the wavelength scale. We identify BCSs in such a structured resonator solving Maxwell's equations directly. The substantial narrowing of the solitons close to the zero-diffraction regime is explained in Sect. 7 by means of a Bloch mode based mean-field model developed in Sect. 3. The paper is concluded in Sect. 8.

2 Mathematical model for a weak-contrast PPS

We consider a planar nonlinear resonator with a weak-contrast refractive index modulation in longitudinal (z) and in one transverse (x) direction, forming a 2D periodic structure [Fig. 1(a)]. Using the ansatz $E(x, z, t) = \Re[u^+(x, z, t) e^{ik_0 z - i\omega_0 t} + u^-(x, z, t) e^{-ik_0 z - i\omega_0 t}]$ for the electric field, a paraxial traveling-wave model for this sys-

tem can be derived as

$$\begin{aligned} i\left(\frac{1}{v_g}\frac{\partial u^+}{\partial t} + \frac{\partial u^+}{\partial z}\right) + \frac{1}{2k_0}\frac{\partial^2 u^+}{\partial x^2} + V(x, z)u^+ \\ + \xi(|u^+|^2 + 2|u^-|^2)u^+ = 0, \quad (1) \\ i\left(\frac{1}{v_g}\frac{\partial u^-}{\partial t} - \frac{\partial u^-}{\partial z}\right) + \frac{1}{2k_0}\frac{\partial^2 u^-}{\partial x^2} + V(x, z)u^- \\ + \xi(|u^-|^2 + 2|u^+|^2)u^- = 0, \end{aligned}$$

where $u^+(x, z, t)$ and $u^-(x, z, t)$ are the slowly varying amplitudes of the forward and backward propagating plane waves, $k_0 = n\omega_0/c$ is the modulus of the wave vector, v_g is the group velocity, and ω_0 is the operating frequency. For the periodic photonic structure we assume a harmonic modulation $V(x, z) = 4m \cos(q_x x) \cos(q_z z)$ of the refractive index in the resonator. We consider both focusing ($\xi > 0$) and defocussing ($\xi < 0$) Kerr nonlinearities. The longitudinal (z) and transverse (x) coordinates are normalized with respect to $x_0 = \sqrt{l_0/2k_0}$, where l_0 is some normalization constant (typical length).

First we neglect the nonlinear terms of (1). Utilizing the 2D periodicity of the linear potential $V(x, z)$ and applying Bloch's theorem the intracavity field can be expanded in terms of spatial harmonics with a common component of the transverse wave vector k_x as

$$\begin{aligned} u^\pm(x, z) = A^\pm(x, z)e^{\pm ik_z(k_x)z + ik_x x} \\ \times \left(\sum_l \sum_p a_{l,p}(k_x) e^{i(lq_x x \mp pq_z z)} \right). \quad (2) \end{aligned}$$

Here the terms in the sum denote 2D Bloch waves [solutions of the linear part of (1)] with slowly varying envelopes A^\pm . Substituting (2) into (1) for the (forward) propagating wave and considering stationary propagation, we get the coupled set of equations

$$\begin{aligned} k_z(k_x)a_{l,p} = pq_z a_{l,p} \\ - \frac{(k_x + lq_x)^2}{2k_0}a_{l,p} + m \sum a_{l\pm 1, p\pm 1}. \quad (3) \end{aligned}$$

In the limit of vanishing modulation $m \rightarrow 0$ we obtain a set of parabolas for the spatial dispersion relation, $k_z(k_x) = -(2k_0)^{-1}(k_x + lq_x)^2 + pq_z$, all shifted with respect to the basic one by integers of the longitudinal and transverse components of the wave vectors of the index modulation $\mathbf{q} = (lq_x, pq_z)$.

The iso-frequency curves $k_z = f(k_x)$ determine the resonance properties of the resonator filled with the PPS. The resonance condition is $k_z = \pi\eta/L$, where the integer η designates the longitudinal modes, and L is the cavity length.

The left ($z = 0$) and right ($z = L$) resonator mirrors are accounted for by the boundary conditions

$$\begin{aligned} u^+(x, z = 0, t) &= \rho e^{i\Phi/2} u^-(x, z = 0, t) + H e^{iKx}, \\ u^-(x, z = L, t) &= \rho e^{i\Phi/2} u^+(x, z = L, t), \end{aligned} \quad (4)$$

where ρ is the reflection coefficient of the mirrors (for simplicity, we assume two identical mirrors of the cavity), and H is the amplitude of the holding beam. The net phase shift $\Phi = \varphi_0 + 2k_0L$ consists of the phase shifts due the reflection at the mirrors φ_0 and due to propagation of linear waves in the resonator without the modulation $2k_0L$, which is split off the propagation model (1) as a fast oscillating term. Taking into account the boundary conditions (4) the intracavity field amplitude in the linear limit is

$$\begin{aligned} A &= \frac{H}{1 - \rho^2 \exp(i(2k_z L + \Phi))} \\ &\approx \frac{H/(1 - \rho^2)}{1 - i\rho^2(2k_z L + \Phi - 2\pi\eta)/(1 - \rho^2)}. \end{aligned} \quad (5)$$

The approximation (5) describes the amplitude of the intracavity field near the longitudinal resonance η . The resonance condition is $\Phi_{\text{res}} + 2k_z(k_x)L = 2\pi\eta$, for any positive integer η . For a homogeneous cavity and a non-tilted holding beam ($m = 0$ and $k_x = K = 0$) the resonance condition simplifies to $\Phi(\omega_\eta) \equiv 2Ln\omega_\eta/c + \varphi_0 = 2\pi\eta$ giving the resonance frequency of the η th longitudinal resonance as $\omega_\eta = (\pi\eta - \varphi_0/2)c/nL$. The imaginary part of the denominator in (5) describes the normalized effective detuning from the nearest resonance frequency

$$\Delta_{\text{eff}} = 2L\rho^2 \frac{k_z(k_x)}{1 - \rho^2} + \Delta. \quad (6)$$

This effective detuning includes the frequency shift induced by the PPS as well as the frequency detuning of the holding beam from the nearest longitudinal resonance ω_η of the empty (homogeneous) resonator $\Delta = 2L\rho^2(\omega_0 - \omega_\eta)n/c(1 - \rho^2)$. Then setting the effective detuning to zero $\Delta_{\text{eff}} = 0$ we can rewrite the resonance condition using the frequency detuning parameter $\Delta_{\text{res}} = -k_z(k_x)2L\rho^2/(1 - \rho^2)$. That way the presence of the resonator imposes the resonance condition on the longitudinal component of the wave vectors of the Bloch modes. The resonance structure of the resonator filled with PPS resembles the band structure of the PPS itself (see Fig. 2). In accordance with (6), the dispersion relation of the linear waves or resonances in the cavity reflects the dispersion properties of Bloch waves propagating in the photonic structure between the mirrors. We note that not only ω_η but all longitudinal resonances contribute to the resonance structure of the PPS resonator giving rise to several coexisting resonances (see Fig. 2).

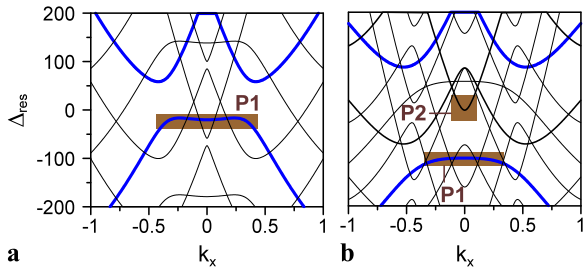


Fig. 2 Linear resonances of the cavity with PPS for two modulations $m = 0.2$ (**a**) and $m = 0.5$ (**b**). The blue-thick lines represent resonances which belong to the same longitudinal modes of the cavity but to different photonic bands, whereas black thick lines correspond to different longitudinal modes. The symbols $P1$, $P2$ designate the areas of photonic bands supporting different types of BCSs. Parameters are: $L = 4.5$, $q_x = 1.571$, $q_z = 1.396$, $\rho = 0.98$

3 Modified mean-field model for Bloch waves for high-contrast photonic crystals

The dielectric distribution in high-contrast PPSs cannot be considered anymore as a weak perturbation of a homogeneous medium, i.e., (1) cannot be used to describe the propagation of light. Instead, envelope equations based on the vectorial Bloch waves as exact solutions of Maxwell's equations can be employed, because, in contrast to the dielectric structure, diffraction and nonlinearity can still be considered as perturbations for wide enough beams and not too large field amplitudes. The equations for the slowly varying envelopes of forward and backward propagating Bloch modes can be derived as (cf. [39–41])

$$\begin{aligned} i\left(\frac{1}{v_g}\frac{\partial A^+}{\partial t} + \frac{\partial A^+}{\partial z}\right) - \frac{1}{2}\frac{\partial^2 k_z}{\partial k_x^2}\frac{\partial^2 A^+}{\partial x^2} + \frac{1}{24}\frac{\partial^4 k_z}{\partial k_x^4}\frac{\partial^4 A^+}{\partial x^4} \\ + \xi_{\text{eff}}(|A^+|^2 + 2|A^-|^2)A^+ = 0, \\ i\left(\frac{1}{v_g}\frac{\partial A^-}{\partial t} - \frac{\partial A^-}{\partial z}\right) - \frac{1}{2}\frac{\partial^2 k_z}{\partial k_x^2}\frac{\partial^2 A^-}{\partial x^2} + \frac{1}{24}\frac{\partial^4 k_z}{\partial k_x^4}\frac{\partial^4 A^-}{\partial x^4} \\ + \xi_{\text{eff}}(|A^-|^2 + 2|A^+|^2)A^- = 0. \end{aligned} \quad (7)$$

Due to their formal similarity to the envelope equations for nonlinear homogeneous media the standard formalism for deriving the mean-field equations for high-finesse planar resonators can be applied. We expect that the essential features and fundamental physics of BCS formation, namely, the interplay between linear dispersion (band structure) and nonlinear effects, can be captured with this simple mean-field model based on Bloch modes.

Applying the corresponding boundary conditions [analogous to (4)] imposed by the mirrors as described in [4] the scaled mean-field equation for the transmitted amplitude

$u(x) = A^+(x, z = L)$ around one of the resonances (ω_{res}) is

$$i\frac{\partial u}{\partial t} + D^{(2)}\frac{\partial^2 u}{\partial x^2} + D^{(4)}\frac{\partial^4 u}{\partial x^4} + \gamma(i + \Delta_{\text{eff}})u + \delta|u|^2u = u_{\text{in}}, \quad (8)$$

where u_{in} the external pump. Deriving this equation the loss γ is given via the relation

$$1/\gamma = \tau_{\text{ph}} = 2L n_g(\omega_{\text{res}}) \rho^2 / c(1 - \rho^2),$$

where τ_{ph} is the photon lifetime in the cavity, L the cavity length, $n_g(\omega)$ the group index inside the cavity, and ρ the reflectivity of the mirrors (in terms of the field amplitudes). The quality factor of the cavity is then $Q = \omega_{\text{res}}\tau_{\text{ph}}/2$. For a given frequency ω_0 the (normalized) detuning from a resonance ω_{res} is defined as $\Delta_{\text{eff}} = \tau_{\text{ph}}(\omega_0 - \omega_{\text{res}}) = 2Q(\omega_0/\omega_{\text{res}} - 1)$. The leading second- and forth-order terms of the dispersion relation are given by

$$D^{(2)} = -\frac{c}{n_g(\omega_{\text{res}})} \frac{\partial^2 k_z}{\partial k_x^2}, \quad (9)$$

$$D^{(4)} = \frac{c}{12n_g(\omega_{\text{res}})} \frac{\partial^4 k_z}{\partial k_x^4}. \quad (10)$$

Note that mean-field equation (8) coincides with the conventional model for the Kerr-nonlinear resonator [1] except for the additional fourth-order diffraction term. Recently similar equations were obtained simulating soliton propagation in arrays of coupled cavities [33] and for an optical microresonator containing an additional left-handed material layer [13].

4 Bloch cavity solitons in a weak-contrast PPS

First, we demonstrate the existence of stable CSs in the framework of the round-trip model (1). Note that a stable CS in the homogeneous cavity is a non-mean-field analog of the well-studied cavity soliton solution in the Lugiato–Lefever model [1]. In accordance with the general theory of CSs, the holding beam frequency has to be detuned slightly below (above) the resonance frequency of the linear dispersive waves of the cavity for a focusing (defocussing) nonlinearity. This means that for the focusing (defocussing) nonlinearity the effective detuning from the corresponding linear resonance Δ_{eff} has to be negative (positive). The local nonlinear shift compensates this detuning leading to a local resonance and to the formation of a stable localized solution. Here we study the localized solutions associated with the bistability of the homogeneous solution ($|\Delta_{\text{eff}}| > \sqrt{3}$). The periodic intracavity index modulation changes the CS shape (both on the large and the small scale) and modifies its existence domain. The CSs now represent the envelopes

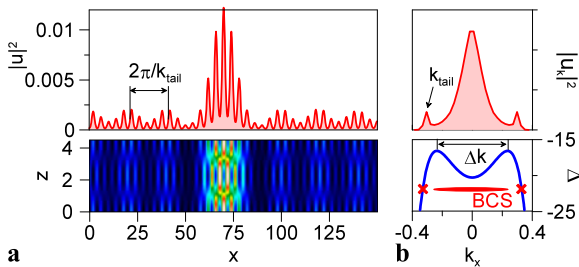


Fig. 3 Bloch cavity soliton bifurcating from the first photonic band depicted by P1 in Fig. 2. (a) Intensity profiles (arb. units) of the bright BCS at the output of the resonator (*upper plot*), and the spatial distributions of the total (forward plus backward) intracavity field (*bottom plot*), calculated by using model (1) for a focusing nonlinearity ($\xi = 1$). (b) Spectrum of BCSs (*upper plot*) and dispersion relation of linear waves (*bottom plots*). Parameters are: $m = 0.2$, $\phi_0 = -0.461$ ($\Delta_{\text{eff}} = -2.5$), $H = 2.45 \cdot 10^{-3}$ and other parameters as in Fig. 2

of the Bloch modes of the corresponding photonic band. The appropriate choice of the operating frequency (Δ) fixes the photonic band of the intracavity PPS. Below we demonstrate several examples of BCSs bifurcating from different photonic bands.

Fundamental photonic band and focusing nonlinearity

Figure 3 shows a typical profile of a stable bright BCS associated with the fundamental (first) photonic band [see domain P1 in Fig. 2(a)]. The dispersion relation of linear waves, i.e. the dependence of their resonance frequency Δ_{res} on the transverse wave vector k_x , deviates drastically from the parabolic shape appearing in homogeneous media in the paraxial approximation. The fourth-order diffraction term plays an important role. As a result the spectrum of the BCS can overlap partially with that of linear dispersive waves leading to their resonant excitation and to the formation of narrow side-resonances ($\pm k_{\text{tail}}$) in the BCS spectrum [Fig. 3(b)]. This resonance radiation has a similar origin as the Cherenkov radiation of solitons in fibers [42] resulting in exponentially decaying spatially oscillating tails of the BCS profile. The major part of the BCS spectrum is confined between two local maxima of the dispersion relation of linear dispersive waves [interval Δk Fig. 3(b)]. Indeed, very narrow BCS will lose much energy due to the radiation into dispersive linear waves until its spectral width becomes smaller than Δk . This value determines the maximal spectral width and thus the minimal size of BCSs for these parameters (see [35]). We will discuss this mechanism in detail below. Note that the BCS remains stable and localized in spite of the fact that the operating frequency belongs to the photonic band of the intracavity PPS. This feature is particular for dissipative solitons (for an example see [33]).

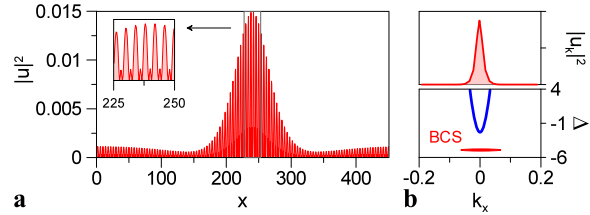


Fig. 4 Intensity profiles (arb. units) (a) and spectrum (b—*top*) of the bright gap Bloch cavity soliton originating from the third photonic band of the PPS and derived from model (1) for a focusing nonlinearity ($\xi = 1$). This BCS exists in the domain depicted by P2 in Fig. 2(b) for the parameters $m = 0.5$, $\phi = -0.138$ ($\Delta_{\text{eff}} = -2.5$) and $H = 3.5 \times 10^{-3}$. Other parameters as in Fig. 2. (b—*bottom*) shows the location of the soliton in the dispersion relation below the third band

Gap Bloch CS existing between the second and the third photonic bands

Tuning the operating frequency slightly below the third photonic band (again $\Delta_{\text{eff}} < -\sqrt{3}$) a gap BCS existing between the second and third photonic band can be excited [see P2 in Fig. 2(b)]. The curvature and, thus, the effective diffraction coefficient ($|D^{(2)}|$) of the dispersion curve associated with the third photonic band is much larger than for the fundamental band. As a result, this BCS is much broader than the BCS associated with the fundamental photonic band (Fig. 4). The inset in Fig. 4(a) shows the Bloch waves associated with the third photonic band in the background of BCSs. Note that similar gap BCSs exist for a defocussing nonlinearity as well. There the BCS bifurcates from the second photonic band.

Fundamental photonic band and defocussing nonlinearity

When the index modulation becomes larger, the resonator diffraction changes its sign and becomes negative [19], and BCSs cease to exist for a focusing nonlinearity [domain depicted by P1 in Fig. 2(b)]. In the opposite (anomalous) diffraction regime, stable bright CSs are possible only for a defocussing nonlinearity ($\xi < 0$), as confirmed by our numerical studies (see Fig. 5). The effective detuning from the corresponding linear resonance $\Delta_{\text{eff}} > \sqrt{3}$ has to be positive for the defocussing case. Several small peaks in the spectrum of this BCSs point out the resonances with the linear dispersive waves and Cherenkov radiation into other photonic bands and longitudinal resonances.

In fact, to observe the diffraction managed solitons in the weak-contrast PPS very long periods of the modulation are required (about 10λ in the transverse and 1000λ in the longitudinal direction). The advantage of the diffraction managed soliton (the possibility to reduce the width), is counteracted by the relatively large scale of the modulation. In order to exploit the diffraction management at most also the modulation should be on the smallest possible spatial scale. This

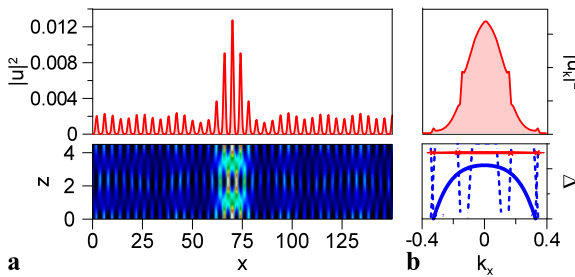


Fig. 5 Intensity profile (arb. units) (a) and spectrum (b—top) of a bright Bloch cavity soliton at the output of the resonator, and the spatial distributions of the total (forward plus backward) intracavity field (bottom plots), calculated from model (1) for a defocusing nonlinearity ($\xi = -1$). This BCS exists in the domain depicted by P1 in Fig. 2(b). Parameters are: $m = 0.5$, $\phi = -1.893$ ($\Delta_{\text{eff}} = 2.5$), the other ones are given in the caption to Fig. 2. (b—bottom) shows the location of the soliton in the dispersion relation above the first band and its interaction with dispersive waves stemming from other bands and other longitudinal resonances

leads to the idea of spatial solitons in resonators with intracavity photonic crystals (PhCs), where the index modulation is on the wavelength scale [Fig. 1(b)]. The direct confirmation of this idea cannot be performed in the frame of the equations for the slowly varying amplitudes (1). In the next paragraph we study the dynamics of light in a nonlinear PhC microresonator (strong modulation with wavelength-scale periodicity) by means of a direct simulation of Maxwell's equations.

5 All-photonic crystal nonlinear resonator

The configuration is displayed in Fig. 1(b). In order to keep the computation time within a reasonable amount, here we consider a 2D effective index distribution of the membrane (air holes in $\varepsilon = 12.25$, radius of the holes is $r = 0.12 \mu\text{m}$, period of the cavity PhC $a = 0.3 \mu\text{m}$ (rotated by 45°), of the mirror PhCs $0.67\sqrt{2}a$ in z direction and $a_x = \sqrt{2}a$ in x direction, cf. also [38, 43]). Apart from possible out-of-plane losses which reduces the quality factor of the cavity results should also hold for a membrane. In our geometry also the mirrors are a photonic crystal. This allows for integrated fabrication and easy tuning of parameters such as the cavity length and mirror reflectivity and thus, the resonance frequencies and quality factor. We consider here the (more complicated) TE-case, i.e., the non-vanishing field components in the (x, z) -plane are E_x , E_z , and H_y .

As mentioned already, instead of using an envelope approach, in the following Maxwell's equations are directly solved without approximation by means of a nonlinear version of the finite-difference time-domain (FDTD) method [44], allowing also for the treatment of structures with strong dielectric modulation.

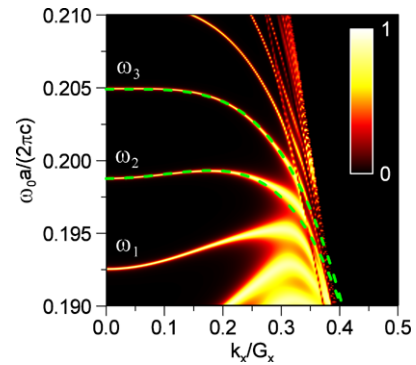


Fig. 6 Transmittance of the linear resonator as shown in Fig. 1(b) as a function of the perpendicular wave vector (in terms of the perpendicular lattice vector $G_x = \sqrt{2}\pi/a$) and the frequency. a is the lattice constant of the interior square lattice PhC [43]. The dashed lines are fourth-order polynomial fits

In the time domain, Maxwell's equations with a Kerr nonlinearity are

$$\begin{aligned} \nabla \times \mathbf{H}(\mathbf{r}, t) &= \frac{\partial \mathbf{D}(\mathbf{r}, t)}{\partial t}, \\ \nabla \times \mathbf{E}(\mathbf{r}, t) &= -\mu_0 \frac{\partial \mathbf{H}(\mathbf{r}, t)}{\partial t}, \\ \mathbf{D}(\mathbf{r}, t) &= \varepsilon_0 \varepsilon(\mathbf{r}) \mathbf{E}(\mathbf{r}, t) + \varepsilon_0 \chi^{(3)}(\mathbf{r}) |\mathbf{E}(\mathbf{r}, t)|^2 \mathbf{E}(\mathbf{r}, t) \end{aligned} \quad (11)$$

where \mathbf{E} and \mathbf{H} are the electric and magnetic fields, ε_0 and μ_0 the permittivity and permeability constants, ε is the relative permittivity, and $\chi^{(3)}$ is the nonlinear coefficient. Note that within the FDTD method, for appropriate initial conditions, the divergence equations are automatically fulfilled for all times. Both the linear and nonlinear response are instantaneous, i.e., material dispersion effects are neglected. Note also that the nonlinear coefficient can be scaled out.

The linear and nonlinear properties of the resonator for plane wave incident fields are described in [38] and [43], respectively. In the latter the occurrence of bistability as a prerequisite for the existence of BCSs is discussed. To have bistability the cavity must be sufficiently detuned from a resonance frequency (see also below). It was shown that self-guiding of the cavity PhC (flat region of the iso-frequency curve) allows for an almost angle-independent bistability for oblique incidence because the cavity detuning for fixed frequency remains almost unchanged [43]. This holds also for the TM-case.

From Fig. 6 three different Fabry-Pérot resonances can be identified: ω_1 , ω_2 , ω_3 (in the following, resonance wavelengths will be given for normal incidence, $k_x = 0$). For these different resonances the photonic crystal changes its dispersion properties, i.e., the dependence of the resonance frequency on the transverse Bloch vector of the intracavity Bloch waves. The first resonance at ω_1 (corresponding to a $\lambda_{\text{res}} = 1.55867 \mu\text{m}$) with a leading second-order term of

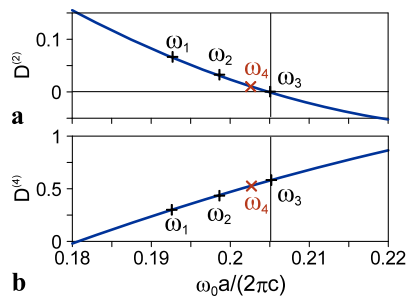


Fig. 7 The effective diffraction coefficients $D^{(2)}$ (**a**) and $D^{(4)}$ (**b**) vs. the normalized frequency. The vertical black line marks the zero-diffraction regime

the dispersion relation complies with the usual cavity (normal diffraction or positive $D^{(2)}$). In the second case, ω_2 , at $\lambda_{\text{res}} = 1.50971 \mu\text{m}$ the next, fourth-order term ($D^{(4)}$) of the dispersion relation has to be included since this term prevails over the second-order term ($D^{(2)}$) for $|k_x/G_x| > 0.1$. For $|k_x/G_x| < 0.1$ the diffraction is normal. In the third case, ω_3 , at $\lambda_{\text{res}} = 1.46416 \mu\text{m}$ the leading term of the dispersion relation is fourth-order (vanishing $D^{(2)}$) with the same sign as in case ω_2 .

Note that the values of the Fabry-Pérot resonances can be tuned by means of a proper design of the resonator length L . Therefore any intermediate values of the operating frequency with desired dispersive properties are accessible. Figure 7 shows the second- ($D^{(2)}$) and fourth- ($D^{(4)}$) order dispersion terms of the intracavity photonic crystal in dependence on the operating frequency.

6 Bloch cavity solitons in all-photonic crystal resonator

In this paragraph we identify different types of BCSs supported by a focusing or defocussing nonlinearity and we prove that extremely small-width solitons can exist. Pumping the cavity homogeneously sufficiently detuned from a resonance frequency and adding a spatio-temporal Gaussian to the pump BCSs can be excited. In our numerical experiments a source is added to H_y . Usually the homogeneous pump amplitude is within a range included in the region of bistability. Since CSs typically have a finite homogeneous plane wave (in our case Bloch wave) background this one has to be stable for them to exist. All non-zero field components of a stable Bloch cavity soliton of case ω_1 are displayed in Fig. 8. BCSs exist in and near the domain of bistability. Adding a sufficiently phase-shifted spatio-temporal Gaussian to the homogeneous pump, the BCS can be erased again.

In Fig. 9(a), (b) the profiles from the introduced mean-field (8) approach are compared to the direct approach for the examples of cases ω_2 and ω_3 . There is excellent agreement between the two approaches, thus confirming that the

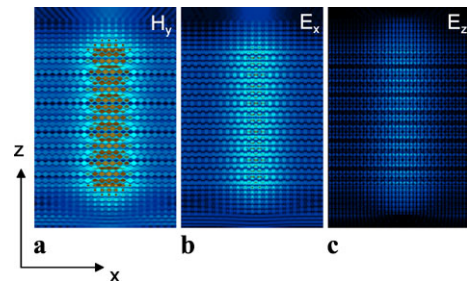


Fig. 8 (**a**) H_y , (**b**) E_x , and (**c**) E_z components of the field of a BCS (case ω_1) for $\Delta_{\text{eff}} = -3$ and $\sqrt{|X^{(3)}|}H_{y,\text{in}} = 0.00022 \text{ A/V}$. Displayed is the absolute value of the fundamental component of the time Fourier series of the real field amplitudes. The computing window comprises 99 periods $\sqrt{2}a$ in x direction

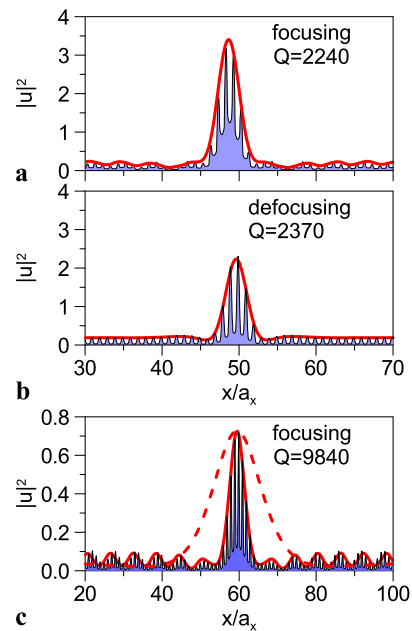


Fig. 9 Comparison of BCSs from the direct approach (black filled line, slice along the x direction within the cavity) and the mean field model (red thick line). Scaling refers to the latter one ($a_x = \sqrt{2}a$). (**a**) case ω_2 for $\Delta_{\text{eff}} = -3$, (**b**) case ω_3 for $\Delta_{\text{eff}} = 3$, and (**c**) case ω_4 for $\Delta_{\text{eff}} = -3$. The dashed line in (**c**) is a solution of the homogeneous cavity

mean-field approach can be used also for PhCs with a large modulation, provided that it is based on Bloch modes. As discussed in Sect. 4 the fourth-order diffraction term leads to radiating tails similar to Cherenkov radiation [cf. Fig. 9(a)] caused by resonant linear coupling (see also [35]).

Because in the third case, ω_3 , at $\lambda_{\text{res}} = 1.46416 \mu\text{m}$, the leading term of the dispersion relation is fourth-order (anomalous fourth-order diffraction), to have cavity solitons the nonlinearity has to be defocussing [cf. Fig. 9(b)]. In case ω_3 self-guiding of the cavity PhC is optimal. As mentioned above, particularly here there is a wide range of bistability for fixed detuning increasing the angle of incidence. This range applies likewise to the constancy of the cavity qual-

ity factor. The width of the resonances corresponds to quality factors $Q = 2240$ (ω_2) and $Q = 2370$ (ω_3) (see Fig. 6). The quality factors can be adjusted easily adding and removing rows of holes to and from the PhC mirrors. The minimum time to excite a BCS (decay of transient oscillations) is around 10 ps. Unlike in the mean-field model the switching time can be read off directly from the simulation.

An important issue, e.g., for possible applications, are the pump power and the width of BCS. Both should be as small as possible. To have a small external pump intensity I_p the quality factor has to be large ($I_p \sim 1/T Q^2$ with the single mirror intensity transmissivity T). But on the other hand, for the purpose of fast all-optical switching, the photon lifetime and thus the quality factor should be small. The dependence here is only linear. Assuming for instance a maximum acceptable photon lifetime $\tau_{ph} = 15$ ps (switching frequency of order 0.1 THz) corresponds to a quality factor around $Q = 10000$.

Toward a more optimal design of our all-PhC cavity we proceed as follows. First, adding two rows of holes to the PhC mirrors of the resonator increases the quality factor of the cavity to $Q = 9840$. Second, the cavity length L is increased by adding one row of holes. This shifts the resonance frequency and hence, changes the diffraction from anomalous to normal, with a small leading second-order term retaining the self-guiding mechanism. We refer to this design with resonance wavelength $\lambda_{res} = 1.47912$ μm as case ω_4 . In Fig. 9(c) a BCS solution of the direct approach is compared to the mean-field model and the homogeneous cavity. It can be seen that compared to the homogeneous cavity case (dashed line) the soliton is significantly narrower. We note that this width corresponds to the free-space wavelength. The amplitude of the switching pulse is of the same order as the plane wave pump. But due to the high Q the switching time in case ω_4 is four times higher than in case ω_2 .

In the direct approach it is easy to determine the pump power. Here the fields are scaled in terms of $\sqrt{|\chi^{(3)}|}$. For the optimal case ω_4 of Fig. 9(c) for example the amplitude of the incident plane wave is around $H_{y,in} = 3.8 \times 10^{-5}/\sqrt{|\chi^{(3)}|}$ A/V. From this the time averaged longitudinal Poynting vector (pump intensity) is $I_p = \langle S_z \rangle = \sqrt{\mu_0/(\epsilon_0 \epsilon)} H_{y,in}^2/2$. For the compound semiconductor GaAs with $\chi^{(3)} = 1.4 \times 10^{-18}$ $\text{m}^2 \text{V}^{-2}$ this gives $I_p = 5.5$ MW cm $^{-2}$. For an experimental realization in an air-suspended membrane of a thickness of 0.3 μm for a sufficiently broad Gaussian (10 solitons widths) pump beam a power of several 100 mW is required.

7 Width of Bloch cavity solitons

A high-quality factor cavity allows for low-threshold nonlinear effects. However, it exhibits relatively large net diffrac-

tion resulting in a large width of BCSs. In this section we present a comprehensive study of the BCS width depending on the normalized operating frequency ($\omega_0 a/(2\pi c) = a/\lambda$). The operating frequency fixes the effective diffraction/dispersion properties of the propagating Bloch waves (see Fig. 7) and, as a consequence, determines the spatial profile of the BCSs. To get a deeper insight into the underlying physics and in order to develop some analytical approximations we will use the modified mean-field model (8). Such analysis was done already for the BCS's width in the case of the weak-contrast PPS resonator [35]. Note that using a similar model Gelens et al. [13] investigated the minimal size of spatially localized solutions in an optical microresonator containing a metamaterial layer. They approximated the CS width as a period length of a spatially periodic pattern forming on a modulationally unstable homogeneous background. This analysis is especially well suited for CSs bifurcating from the edge of modulational instability of a homogeneous solution in the monostable regime ($|\Delta_{eff}| < \sqrt{3}$). Here we consider the localized solution coexisting with bistability of the homogeneous solution ($|\Delta_{eff}| > \sqrt{3}$).

The existence of bright BCSs in the focusing case ($\delta > 0$) with negative cavity detuning ($\Delta_{eff} < -\sqrt{3}$) is evident for small frequencies where the parabolic term ($D^{(2)}$) is the leading diffraction term (Fig. 7). For an increasing operating frequency the BCSs become narrower (see Fig. 10). Indeed the effective net diffraction of the cavity $D^{(2)}$ decreases with increasing frequency ω_0 , and even changes the sign after the inflection point (vanishing $D^{(2)}$). If the parabolic term is the leading one for the net diffraction, the BCS width simply scales with the square root of the effective second-order

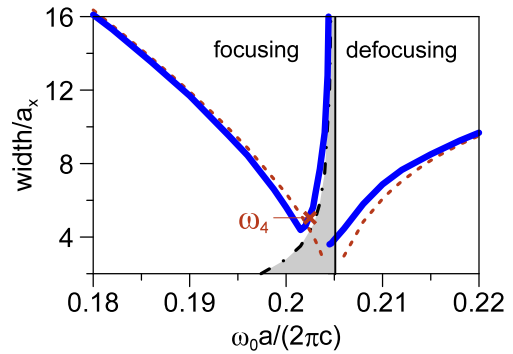


Fig. 10 The width of BCSs (normalized to the value a_x) vs. normalized frequency for $Q = 9840$. The vertical black line marks the zero-diffraction regime. Far from this zero-diffraction point the BCS width scales with the effective second-order diffraction coefficient (12) depicted by red dashed lines. In accordance with (13) the dashed dotted (black) line depicts the minimal soliton width. The region left of the zero-diffraction regime corresponds to normal diffraction and focusing nonlinearity: $\delta = 1$ for $\Delta_{eff} = -3$. The region to the right is the case of anomalous (inverted) diffraction and defocusing nonlinearity: $\delta = -1$ for $\Delta_{eff} = 3$

diffraction coefficient as

$$W(\omega_0) = W_0 \sqrt{|D^{(2)}(\omega_0)|Q}, \quad (12)$$

where W_0 is some normalization value. As the photon lifetime, the width of cavity solitons also increases with Q . Relation (12) confirms that the BCS width should decrease with increasing ω_0 (in the focusing region) and gives a good estimate for small frequencies ω_0 (Fig. 10). Note that similar to conventional CSs (see for instance [12, 13]) the BCS width depends on the effective cavity detuning Δ_{eff} which scales with the distance of the operating frequency to the nearest resonance frequency. Therefore, in Fig. 10 we depict the dependence of the BCS width (“full width at half maximum”—FWHM) on the frequency keeping the effective cavity detuning Δ_{eff} fixed (by changing the cavity to readjust the cavity resonance).

The approximation of (12) fails as soon as the next-order (fourth-order) diffraction term plays a significant role for the formation of the BCS profile. As a result the BCS width attains a minimum not exactly at the zero-diffraction (inflection) point but for essentially smaller frequency (Fig. 10). Indeed, due to the interplay between second- and fourth-order diffraction the dispersion relation possesses two maxima at symmetric transverse wave vectors. As was shown in the weak-contrast case [35], the maximal spectral width of BCS has to be bound between two maxima because of the strong Cherenkov radiation. Due to the resonance between BCS and linear modes the BCS tails are modulated on a large transverse extension [see Fig. 9(a), (c)]. As a result the minimal width of the BCSs accessible for the given PPS can be approximated by the relation

$$W_{\min}(\omega_0) \approx 4 \cdot \ln 2 \sqrt{2D^{(4)}(\omega_0)/D^{(2)}(\omega_0)}. \quad (13)$$

This mechanism (13) explains the sharp growth of the BCS width in the vicinity of the zero-diffraction point and that BCSs cease to exist for $D^{(2)} \rightarrow 0$ (Fig. 10). Note that the bifurcation analysis of periodic patterns gives similar results for the typical size of localized structures [13].

The whole picture changes qualitatively beyond the zero-diffraction point, where the effective (second-order) diffraction changes its sign [as evident from the dispersion curves in Fig. 7(a)]. Bright BCSs cease to exist for a focusing nonlinearity just before the zero-diffraction point, however, they reappear for a defocusing nonlinearity and positive effective cavity detuning. The substantial reduction of the BCS width can be seen in Fig. 10. If the fourth-order $D^{(4)}$ diffraction term is leading the BCS width simply scales as

$$W(\omega_0) = W_0 \sqrt[4]{D^{(4)}(\omega_0)Q}. \quad (14)$$

But here the cavity filled with a nonlinear PhC has an advantage. For a cavity filled with a homogeneous nonlinear material the scaling of the width in terms of Q is like $\sqrt[4]{Q}$. In the

defocusing case ω_3 it scales only like $\sqrt[4]{Q}$ which is due to self-guiding. The second-order diffraction term determines the width and the shape of the BCSs sufficiently far from the zero-diffraction point and, therefore, the BCS width can be estimated again by (12) ($D^{(2)}(\omega_0) < 0$). Note that unlike in the case of normal diffraction the defocusing nonlinearity supports bright BCSs even at the zero-diffraction point (vertical line in Fig. 10).

8 Conclusions

In conclusion, we investigated different types of Bloch cavity solitons in nonlinear resonators with a genuine 2D periodic modulation of the refractive index. The coexistence of solitons bifurcating from different Bloch dispersion branches was shown. In order to analyze the properties of the BCS and to gain analytical insight we developed a modified mean-field model for a weak-contrast intracavity PPS, based on the paraxial round-trip model. We analyzed the properties of BCS in the vicinity of the zero-diffraction regime. In particular, bright BCSs become infinitely broad close to the zero-diffraction point for a focusing nonlinearity, whereas a defocusing nonlinearity supports narrow BCS. We identified branches of Bloch cavity solitons in an all-photonic crystal resonator for different types of resonances solving Maxwell's equations directly. The validity of a mean-field model based on Bloch modes was confirmed even for a large modulation of the PhC. Width and pump power of the BCSs were optimized adjusting the quality factor and the length of the cavity.

Acknowledgements This work was supported by the Deutsche Forschungsgemeinschaft (research unit 532).

References

1. L.A. Lugiato, R. Lefever, Phys. Rev. Lett. **58**, 2209 (1987)
2. V.B. Taranenko, K. Staliunas, C.O. Weiss, Phys. Rev. Lett. **81**, 2236 (1998)
3. V.B. Taranenko, I. Ganne, R. Kuszelewicz, C.O. Weiss, Phys. Rev. A **61**, 063818 (2000)
4. D. Michaelis, U. Peschel, C. Etrich, F. Lederer, IEEE J. Quantum Electron. **39**, 255 (2003)
5. D. Michaelis, U. Peschel, F. Lederer, Phys. Rev. A **56**, 3366(R) (1997)
6. M. Brambilla, L.A. Lugiato, F. Prati, L. Spinelli, W.J. Firth, Phys. Rev. Lett. **79**, 2042 (1997)
7. N.N. Rosanov, *Spatial Hysteresis and Optical Patterns* (Springer, Heidelberg, 2002)
8. U. Peschel, D. Michaelis, C. Weiss, IEEE J. Quantum Electron. **39**, 51 (2003)
9. S. Barland, J. Tredicce, M. Brambilla, L. Lugiato, S. Balle, M. Giudici, T. Maggipinto, L. Spinelli, G. Tissoni, T. Knödl, M. Miller, R. Jäger, Nature **419**, 699 (2002)
10. T. Ackemann, W.J. Firth, G. Oppo, Adv. At. Mol. Opt. Phys. **57**, 324 (2009)

11. N. Akhmediev, A. Ankiewicz, *Dissipative Solitons* (Springer, Berlin, 2005)
12. P. Kockaert, P. Tassin, G.V. der Sande, I. Veretennicoff, M. Tlidi, Phys. Rev. A **74**, 033822 (2006)
13. L. Gelens, G.V. der Sande, P. Tassin, M. Tlidi, P. Kockaert, D. Gomila, I. Veretennicoff, J. Danckaert, Phys. Rev. A **75**, 063812 (2007)
14. D.N. Christodoulides, F. Lederer, Y. Silberberg, Nature **424**, 817 (2003)
15. F. Lederer, G.I. Stegeman, D.N. Christodoulides, G. Assanto, M. Segev, Y. Silberberg, Phys. Rep. **463**, 1 (2008)
16. Y.S. Kivshar, G.P. Agrawal, *Optical Solitons: From Waveguides to Photonic Crystals* (Academic Press, San Diego, 2003)
17. H. Kosaka, T. Kawashima, M. Tomita, M. Notomi, T. Tamamura, T. Sato, S. Kawakami, Appl. Phys. Lett. **74**, 1212 (1999)
18. R. Iliew, C. Etrich, U. Peschel, F. Lederer, M. Augustin, H.-J. Fuchs, D. Schelle, E.-B. Kley, S. Nolte, A. Tünnermann, Appl. Phys. Lett. **85**, 5854 (2004)
19. K. Staliunas, R. Herrero, Phys. Rev. E **73**, 016601 (2006)
20. A.A. Sukhorukov, Y.S. Kivshar, Phys. Rev. Lett. **87**, 083901 (2001)
21. D. Neshev, A.A. Sukhorukov, B. Hanna, W. Krolikowski, Y.S. Kivshar, Phys. Rev. Lett. **93**, 083905 (2004)
22. K. Staliunas, R. Herrero, Phys. Rev. E **73**, 065603(R) (2006)
23. D. Gomila, R. Zambrini, G.L. Oppo, Phys. Rev. Lett. **92**, 253904 (2004)
24. D. Gomila, G.L. Oppo, Phys. Rev. E **72**, 016614 (2005)
25. N. Marsal, D. Wolfersberger, M. Sciamanna, G. Montemezzani, D.N. Neshev, IEEE J. Quantum Electron. **45**, 1380 (2009)
26. U. Peschel, O. Egorov, F. Lederer, Opt. Lett. **29**, 1909 (2004)
27. O. Egorov, F. Lederer, Y.S. Kivshar, Opt. Express **15**, 4149 (2007)
28. O.A. Egorov, F. Lederer, Phys. Rev. A **76**, 053816 (2007)
29. A.G. Vladimirov, D.V. Skryabin, G. Kozyreff, P. Mandel, M. Tlidi, Opt. Express **14**, 1 (2006)
30. A.V. Yulin, D.V. Skryabin, P.S.J. Russell, Opt. Express **13**, 3529 (2005)
31. K. Staliunas, Phys. Rev. Lett. **91**, 053901 (2003)
32. K. Staliunas, Phys. Rev. E **70**, 016602 (2004)
33. O. Egorov, F. Lederer, K. Staliunas, Opt. Lett. **32**, 2106 (2007)
34. K. Staliunas, O. Egorov, Y.S. Kivshar, F. Lederer, Phys. Rev. Lett. **101**, 153903 (2008)
35. O.A. Egorov, F. Lederer, K. Staliunas, Phys. Rev. A **82**, 043830 (2010)
36. K. Staliunas, M. Peckus, V. Sirutkaitis, Phys. Rev. A **76**, 05183(R) (2007)
37. M. Peckus, R. Rogalskis, M. Andrulevicius, T. Tamulevicius, A. Guobiene, V. Jarutis, V. Sirutkaitis, K. Staliunas, Phys. Rev. A **79**, 033806 (2009)
38. R. Iliew, C. Etrich, T. Pertsch, F. Lederer, K. Staliunas, Opt. Lett. **33**, 2695 (2008)
39. N.A.R. Bhat, J.E. Sipe, Phys. Rev. E **64**, 056604 (2001)
40. K. Busch, M. Frank, A. Garcia-Martin, D. Hermann, S.F. Mingaleev, M. Schillinger, L. Tkeshelashvili, Phys. Status Solidi A **197**, 637 (2003). <http://dx.doi.org/10.1002/pssa.200303111>
41. R. Iliew, C. Etrich, T. Pertsch, F. Lederer, Phys. Rev. B **77**, 115124 (2008)
42. N. Akhmediev, M. Karlsson, Phys. Rev. A **51**, 2602 (1995)
43. R. Iliew, C. Etrich, F. Lederer, K. Staliunas, Opt. Lett. **35**, 3907 (2010)
44. A. Taflove, S.C. Hagness, *Computational Electrodynamics: The Finite-Difference Time-Domain Method* (Artech House, Boston, 2000)